Leaky Rayleigh and Scholte waves at the fluid–solid interface subjected to transient point loading

Jinying Zhu and John S. Popovics[a)]
Department of Civil and Environmental Engineering, University of Illinois at Urbana, Illinois 61801

Frank Schubert
Lab EADQ, Fraunhofer Institute for Nondestructive Testing, D-01326 Dresden, Germany

(Received 6 February 2004; revised 9 July 2004; accepted 18 July 2004)

The analysis of acoustic waves generated by a transient normal point load applied on a fluid–solid interface is presented. The closed-form exact solution of the wave motion is obtained by using integral transform techniques. The obtained analytical solution provides necessary theoretical background for optimization of fluid-coupled ultrasonic and acoustic wave detection in experiments. Numerical simulation (elastodynamic finite integration technique) is performed to verify the obtained analytical solution. Detailed descriptions of leaky Rayleigh and Scholte wave solutions are presented. A simplified solution to isolate the contributions of leaky Rayleigh and Scholte waves generated by a transient point load is proposed, and closed-form formulations for displacement and stress components are then presented. The simplified solution is compared to the exact solution for two configurations: water/concrete and air/concrete. The excitation effectiveness of leaky Rayleigh waves for the air/concrete configuration is studied, which has practical significance to air-coupled sensing in civil engineering structures.
[DOI: 10.1121/1.1791718]

PACS numbers: 43.35.Pt, 43.20.El, 43.35.Zc [YHB] Pages: 2101–2110

I. INTRODUCTION

The propagating leaky Rayleigh wave that emanates from a fluid–solid interface has been used as an effective means for surface and subsurface defect detection. With recent improvements in instrumentation, air-coupled transducers have been used for detection of leaky surface (Zhu *et al.*, 2001) and leaky guided waves (Castaings *et al.*, 2001). With the advantage of noncontact sensing, air-coupled transducers provide an opportunity for quick scanning and imaging of large civil engineering structures by detecting the leaky Rayleigh wave. Therefore, detailed study of leaky surface waves for this case is needed.

Extensive studies and applications of leaky surface waves have been reported during the past 40 years. A comprehensive study of Rayleigh waves and leaky Rayleigh waves has been given by Viktorov (1967), where leaky Rayleigh waves at the interfaces of a solid half-space with both a fluid layer and a fluid half-space were investigated in great detail. Leaky Rayleigh waves propagate with a velocity slightly higher than the ordinary Rayleigh wave, and attenuate more intensively with distance due to continuous energy radiation into the fluid. It was initially believed that the leaky Rayleigh wave exists when the fluid wave velocity c_F is smaller than the leaky Rayleigh wave velocity c_{LR}. However, Mozhaev and Weihnacht (2002) showed the actual threshold phase velocity for leaky Rayleigh wave existence was 1.45% lower than the acoustic wave velocity of the fluid. The character and existence conditions of leaky Rayleigh and Scholte waves were also investigated experimentally by Glorieux *et al.* (2001). The propagation of leaky Rayleigh waves under the influences of viscous damping and heat conduction at the fluid–solid interface was studied by Qi (1994), who concluded that the effect of viscosity can be neglected for fluids with Reynolds number larger than 2500. For common fluids such as water and air at normal driving frequencies (<10 MHz), the viscous effect of the fluid can be neglected because the Reynolds numbers are far above the critical value of 2500.

The response of leaky waves owing to transient point loading is of great practical interest to nondestructive evaluation (NDE) researchers, especially in civil engineering, where an impulse hammer or a point impactor applied to the surface of the solid is often used as a transient wave source. Gusev *et al.* (1996) provided detailed theoretical analyses of laser-induced wave motions at the fluid–solid interface, which include Scholte, leaky Rayleigh, and lateral waves. General solutions for interface wave motion were given using a 2-D formulation. 2-D and 3-D analytical solutions for a fluid–solid configuration subjected to implosive line and point sources in the fluid have been given by de Hoop *et al.* (1983, 1984). However, for the case of the ''Lamb'' problem in fluid–solid configuration, where a normal transient point load is applied at the fluid–solid interface, no closed-form exact solution has been reported so far.

In this paper, Laplace and Hankel integral transforms are employed to derive the full analytical solution to the ''Lamb'' problem in a fluid–solid half-space system, where a point load, varying with time as a step function, is applied at the interface. The obtained step response solution is shown in integral format, which can be calculated numerically. Impulse responses are then obtained by differentiating the step responses. Therefore, for any transient impact loading that

[a)]Author to whom correspondence should be addressed. Electronic mail: johnpop@uiuc.edu

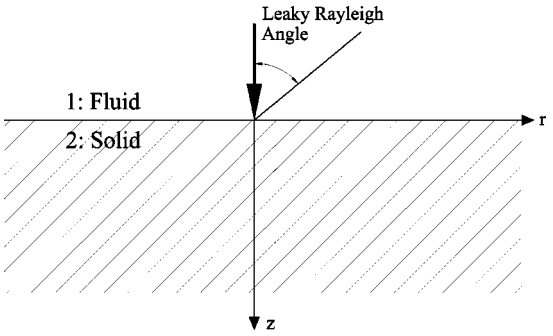

FIG. 1. A transient point load applied at the interface of a fluid–solid half-space system.

has arbitrary temporal variation and spatial distribution, the responses can be obtained by convolving the impulse response in time and space domains. The obtained analytical solutions are verified by EFIT (elastodynamic finite integration technique) numerical simulation, which is a powerful tool for elastodynamic wave field analysis. Then a simplified analytical formulation for the pressure field in the fluid is derived and illustrated.

II. COMPLETE FORMULATION

Consider a fluid–solid half-space system as shown in Fig. 1. The solid half-space is given by $z>0$, and the fluid by $z<0$. The properties of the fluid are given by the Lamé constant λ_1 and mass density ρ_1, and those of the solid by the Lamé constants λ_2 and μ and density ρ_2. The interface between the fluid and solid half-space is subjected to a normal point load of magnitude $QH(t)$, where $H(t)$ is the Heaviside step function. Because the wave motion in the fluid and solid generated by the point load is axially symmetric about the z axis, cylindrical coordinates are employed, where the origin is located at the load point on the interface.

A. Fluid–solid half-space

Introducing displacement potential functions φ_1 in the fluid and φ_2 and ψ in the solid, the governing equations for the fluid and the solid half-spaces are

$$\begin{aligned}
&\frac{\partial^2\varphi_1}{\partial r^2}+\frac{1}{r}\frac{\partial\varphi_1}{\partial r}+\frac{\partial^2\varphi_1}{\partial z^2}=\frac{1}{c_F^2}\ddot{\varphi}_1,\\
&\frac{\partial^2\varphi_2}{\partial r^2}+\frac{1}{r}\frac{\partial\varphi_2}{\partial r}+\frac{\partial^2\varphi_2}{\partial z^2}=\frac{1}{c_P^2}\ddot{\varphi}_2,\\
&\frac{\partial^2\psi}{\partial r^2}+\frac{1}{r}\frac{\partial\psi}{\partial r}+\frac{\partial^2\psi}{\partial z^2}-\frac{\psi}{r^2}=\frac{1}{c_S^2}\ddot{\psi},
\end{aligned} \tag{1}$$

where $c_F^2=\lambda_1/\rho_1$ is the acoustic wave velocity in the fluid, and $c_P^2=(\lambda_2+2\mu)/\rho_2$ and $c_S^2=\mu/\rho_2$ are the P- and S-wave velocities in the solid. The double dots represent a double derivative with respect to time. The displacements are related to potential functions by

$$u_1=\frac{\partial\varphi_1}{\partial r},\quad w_1=\frac{\partial\varphi_1}{\partial z},$$

$$u_2=\frac{\partial\varphi_2}{\partial r}-\frac{\partial\psi}{\partial z},\quad w_2=\frac{\partial\varphi_2}{\partial z}+\frac{1}{r}\frac{\partial(r\psi)}{\partial r}, \tag{2}$$

where the subscripts 1 and 2 represent quantities related to the fluid and solid, respectively.

B. Continuity and initial condition

A point load is applied at the origin as a Dirac delta function in space and varies as a Heaviside step function in time, which can be expressed as $QH(t)\delta(r)/2\pi r$. Because ideal fluid and shear-free interface conditions are assumed, only the normal stress and vertical component of the displacement are continuous at the interface. The continuity conditions at $z=0$ are

$$\begin{aligned}
&w_1=w_2,\\
&\tau_{zz2}=\tau_{zz1}+(-Q)H(t)\frac{\delta(r)}{2\pi r}=-P-QH(t)\frac{\delta(r)}{2\pi r},\\
&\tau_{zr2}=\tau_{zr1}=0,
\end{aligned} \tag{3}$$

where τ_{zz} and τ_{zr} are the normal and shear components of stress, and P the pressure in the fluid.

Assuming the system is at rest prior to $t=0$, we have

$$\begin{aligned}
\varphi_1(r,z,0)&=\ddot{\varphi}_1(r,z,0)\\
&=\varphi_2(r,z,0)=\ddot{\varphi}_2(r,z,0)\\
&=\psi_2(r,z,0)=\ddot{\psi}_2(r,z,0)=0.
\end{aligned} \tag{4}$$

C. Integral transform

One-sided Laplace and Hankel transforms are used to obtain solutions to the equations. The Laplace and nth-order Hankel transforms are defined respectively as

$$\overline{f}(p)=\int_0^\infty f(t)e^{-pt}\,dt,\quad f^{H_n}(\xi)=\int_0^\infty f(r)J_n(\xi r)r\,dr, \tag{5}$$

where p and ξ are variables of the Laplace and Hankel transforms, respectively.

Applying the Laplace transform to Eq. (1) with respect to time t and the zeroth- and first-order Hankel transform with respect to the radial distance r yields

$$\begin{aligned}
&\frac{d^2\overline{\varphi}_1^{H_0}}{dz^2}-\alpha_1^2\overline{\varphi}_1^{H_0}=0,\\
&\frac{d^2\overline{\varphi}_2^{H_0}}{dz^2}-\alpha_2^2\overline{\varphi}_2^{H_0}=0,\quad \frac{d^2\overline{\psi}^{H_1}}{dz^2}-\beta^2\overline{\psi}^{H_1}=0,
\end{aligned} \tag{6}$$

where

$$\alpha_1^2=\xi^2+s_F^2p^2,\quad \alpha_2^2=\xi^2+s_P^2p^2,\quad \beta^2=\xi^2+s_S^2p^2, \tag{7}$$

and s_F, s_P, s_S are P- and S-wave slowness in the fluid and the solid. Only choosing the terms which lead to finite responses for large values of $|z|$, we obtain the solutions to Eq. (6),

$$\bar{\varphi}_1^{H_0}=\Phi_1(\xi,p)e^{\alpha_1 z},$$

$$\bar{\varphi}_2^{H_0}=\Phi_2(\xi,p)e^{-\alpha_2 z},\quad \bar{\psi}^{H_1}=\Psi(\xi,p)e^{-\beta z}, \tag{8}$$

where $\Phi_1(\xi,p)$, $\Phi_2(\xi,p)$, and $\Psi(\xi,p)$ are functions of p and ξ that need to be determined. From Eq. (2) and the displacement–stress relationships, the transformed displacements and stresses (pressure for the fluid) in the fluid are

$$\bar{w}_1^{H_0}=\frac{d\bar{\varphi}_1^{H_0}}{dz},\quad \bar{u}_1^{H_1}=-\xi\bar{\varphi}_1^{H_0},\quad \bar{P}^{H_0}=-\rho_1 p^2\bar{\varphi}_1^{H_0}, \tag{9}$$

and in the solid are

$$\bar{w}_2^{H_0}=\frac{d\bar{\varphi}_2^{H_0}}{dz}+\xi\bar{\psi}^{H_1},\quad \bar{u}_2^{H_1}=-\frac{d\bar{\psi}^{H_1}}{dz}-\xi\bar{\varphi}_2^{H_0},$$

$$\bar{\tau}_{zz2}^{H_0}=\mu\left[(s_S^2p^2+2\xi^2)\bar{\varphi}_2^{H_0}+2\xi\frac{d\bar{\psi}^{H_1}}{dz}\right], \tag{10}$$

$$\bar{\tau}_{zr2}^{H_1}=-\mu\left[2\xi\frac{d\bar{\varphi}_2^{H_0}}{dz}+(s_S^2p^2+2\xi^2)\bar{\psi}^{H_1}\right].$$

Applying the same integral transforms to the continuity conditions Eq. (3), then substituting Eqs. (9) and (10) into it, generates a group of linear equations in terms of $\Phi_1(\xi,p)$, $\Phi_2(\xi,p)$, and $\Psi(\xi,p)$. Solving the equations yields

$$\Phi_1=\frac{Q}{2\pi\mu p}\frac{\alpha_2}{\alpha_1}\frac{s_S^2p^2}{D_H(\xi,p)},\quad \Phi_2=-\frac{Q}{2\pi\mu p}\frac{s_S^2p^2+2\xi^2}{D_H(\xi,p)},$$

$$\Psi=-\frac{Q}{2\pi\mu p}\frac{2\alpha_2\xi}{D_H(\xi,p)}, \tag{11}$$

where

$$D_H(\xi,p)=(s_S^2p^2+2\xi^2)^2-4\xi^2\alpha_2\beta+\frac{\rho_1}{\rho_2}p^4s_S^4\frac{\alpha_2}{\alpha_1}. \tag{12}$$

Substituting Eq. (11) into Eqs. (9) and (10), we obtain the displacements and pressure in the fluid,

$$\bar{w}_1^{H_0}=\frac{Q}{2\pi}\frac{1}{\mu}\frac{\alpha_2 s_S^2p}{D_H(\xi,p)}e^{\alpha_1 z},$$

$$\bar{u}_1^{H_1}=-\frac{Q}{2\pi}\frac{1}{\mu}\frac{\alpha_2}{\alpha_1}\frac{s_S^2p\xi}{D_H(\xi,p)}e^{\alpha_1 z}, \tag{13}$$

$$\bar{P}^{H_0}=-\frac{Q}{2\pi}\frac{\rho_1}{\rho_2}\frac{\alpha_2}{\alpha_1}\frac{s_S^4p^3}{D_H(\xi,p)}e^{\alpha_1 z},$$

and the displacements and stresses in the solid

$$\bar{u}_2^{H_1}=\frac{Q}{2\pi}\frac{1}{\mu p}[(s_S^2p^2+2\xi^2)e^{-\alpha_2 z}-2\alpha_2\beta e^{-\beta z}]\frac{\xi}{D_H(\xi,p)},$$

$$\bar{w}_2^{H_0}=\frac{Q}{2\pi}\frac{1}{\mu p}[(s_S^2p^2+2\xi^2)e^{-\alpha_2 z}-2\xi^2e^{-\beta z}]\frac{\alpha_2}{D_H(\xi,p)}, \tag{14}$$

$$\bar{\tau}_{zz2}^{H_0}=-\frac{Q}{2\pi}\frac{1}{p}[(s_S^2p^2+2\xi^2)^2e^{-\alpha_2 z}-4\alpha_2\beta\xi^2e^{-\beta z}]\frac{1}{D_H(\xi,p)},$$

$$\bar{\tau}_{zr2}^{H_1}=\frac{Q}{2\pi}\frac{1}{p}[-e^{-\alpha_2 z}+e^{-\beta z}]\frac{2\alpha_2\xi(s_S^2p^2+2\xi^2)}{D_H(\xi,p)}.$$

III. CHARACTERISTIC EQUATION FOR LEAKY RAYLEIGH AND SCHOLTE WAVES

$D_H(\xi,p)=0$ is the characteristic equation for leaky Rayleigh waves at the interface of fluid–solid half-spaces. Introducing the substitution $\gamma=i\xi/ps_S$ and notations $q=s_L/s_S$ and $u=s_F/s_S$, the equation $D_H=0$ can be changed to the following in terms of γ:

$$(1-2\gamma^2)^2-4\gamma^2\sqrt{\gamma^2-1}\sqrt{\gamma^2-q^2}+\frac{\rho_1}{\rho_2}\frac{\sqrt{\gamma^2-q^2}}{\sqrt{\gamma^2-u^2}}=0. \tag{15}$$

Equation (15) is the same as that given by Viktorov (1967), which differs from the regular Rayleigh equation in the third term due to the pressure of the fluid. Equation (15) produces eight Riemann sheets owing to the square roots. The roots have the physical meaning of normalized slowness with respect to s_S. When leaky Rayleigh waves exist, we can obtain six roots, which include two pairs of complex conjugate pairs corresponding to the leaky Rayleigh wave $[\mathrm{Re}(\gamma_R^2)<u^2]$, and two opposite real roots corresponding to the Scholte wave $(\gamma_{sch}^2>u^2)$.

The two pairs of complex conjugate roots corresponding to the leaky Rayleigh wave take the form of $\pm[\mathrm{Re}(\gamma)\pm i\,\mathrm{Im}(\gamma)]$, in which only two roots are acceptable. Because p is the Laplace transform variable, $\mathrm{Re}(p)$ must be negative to have a finite time domain response. Therefore, only the roots which lead to $\mathrm{Re}(p)<0$ are acceptable, where $p=i\xi/\gamma s_S$. A quick analysis shows that the two acceptable roots take the form of $\gamma_{R1,R2}=\pm\mathrm{Re}(\gamma)-i\,\mathrm{Im}(\gamma)$. Here, we denote them as γ_{R1}, γ_{R2}, and note $\gamma_{R2}=-\bar{\gamma}_{R1}$, where the top bar indicates complex conjugate.

Analysis also shows that $|\mathrm{Re}(\gamma_{R1,R2})|<s_R/s_S$, where s_R is the slowness of Rayleigh wave in free surface solid half-space. This result confirms that the slowness of the leaky Rayleigh wave is smaller than s_R, i.e., in a fluid–solid half-space system, the leaky Rayleigh wave will travel faster than the pure Rayleigh wave in the same free surface solid. This conclusion is reasonable considering the influence of fluid pressure applied on solid surface. The imaginary part of γ_R accounts for the energy leaked into fluid. The larger the value of $|\mathrm{Im}(\gamma_{R1})|$, the more energy leaks into the fluid.

The Scholte wave velocity can be obtained from the real roots $\pm\gamma_{sch}$, where $\gamma_{sch}>u$ and $s_{sch}=\gamma_{sch}s_S$. Scholte waves always exist for any fluid–solid combination case. For the lighter fluids lying on stiffer solids case, s_{sch} is only slightly smaller than the acoustic wave velocity of the fluid, and the Scholte wave contribution is relatively small. The property of Scholte waves will be discussed in more detail in Sec. VII.

IV. SOLUTION OF PRESSURE IN THE FLUID

The solution of fluid pressure in the space–time domain is derived because pressure in the fluid is the most often measured quantity in practical application. By taking the inverse zeroth-order Hankel transform to Eq. (13) and introducing the substitution $\xi = p\eta$, we have

$$\overline{P} = -\frac{Qs_S^4}{2\pi}\frac{\rho_1}{\rho_2}\int_0^\infty \frac{\sqrt{\eta^2+s_P^2}}{\sqrt{\eta^2+s_F^2}}\frac{p}{D(\eta)} \times e^{pz\sqrt{\eta^2+s_F^2}} J_0(p\eta r)\,\eta\,d\eta, \tag{16}$$

where $D(\eta)$ is defined as

$$D(\eta) = (2\eta^2+s_S^2)^2 - 4\eta^2\sqrt{\eta^2+s_P^2}\sqrt{\eta^2+s_S^2} + \frac{\rho_1}{\rho_2}\frac{\sqrt{\eta^2+s_P^2}}{\sqrt{\eta^2+s_F^2}}s_S^4. \tag{17}$$

The inverse Laplace transform is evaluated by the Cagniard–de Hoop method, as described by Achenbach (1973). Introducing the following representation of $J_0(x)$,

$$J_0(x) = \frac{2}{\pi}\mathrm{Im}\int_1^\infty \frac{e^{ixs}}{\sqrt{s^2-1}}ds, \tag{18}$$

and substituting it into Eq. (16) yields

$$\overline{P} = -\frac{Qs_S^4}{\pi^2}\frac{\rho_1}{\rho_2}\mathrm{Im}\int_0^\infty \frac{\sqrt{\eta^2+s_P^2}}{\sqrt{\eta^2+s_F^2}}\frac{\eta}{D(\eta)}d\eta \times \int_1^\infty p\frac{e^{ip\eta rs+pz\sqrt{\eta^2+s_F^2}}}{\sqrt{s^2-1}}ds. \tag{19}$$

Introducing the substitution $t = -i\eta rs - z\sqrt{\eta^2+s_F^2}$ and $\eta = iv$ yields

$$\overline{P} = \frac{Qs_S^4}{\pi^2}\frac{\rho_1}{\rho_2}\mathrm{Im}\int_0^{-i\infty}\frac{\sqrt{s_P^2-v^2}}{\sqrt{s_F^2-v^2}}\frac{v}{D(iv)}dv \times \int_1^\infty p\frac{e^{-pt}}{\sqrt{s^2-1}}ds, \tag{20}$$

where

$$L^{-1}\left(\int_1^\infty p\frac{e^{-pt}}{\sqrt{s^2-1}}ds\right) = \frac{d}{dt}\left(\frac{H(t+z\sqrt{s_F^2-v^2}-vr)}{\sqrt{(t+z\sqrt{s_F^2-v^2})^2-v^2r^2}}\right) \tag{21}$$

and L represents the Laplace transform. Therefore, the inverse Laplace transform of Eq. (20) is

$$P(t) = \frac{Qs_S^4}{\pi^2}\frac{\rho_1}{\rho_2}\frac{d}{dt}\left(\mathrm{Im}\int_0^{-i\infty}\frac{\sqrt{s_P^2-v^2}}{\sqrt{s_F^2-v^2}}\frac{v}{D(iv)} \times \frac{H(t+z\sqrt{s_F^2-v^2}-vr)}{\sqrt{(t+z\sqrt{s_F^2-v^2})^2-v^2r^2}}dv\right) = \frac{Qs_S^4}{\pi^2}\frac{\rho_1}{\rho_2}\frac{d}{dt}G^P(t), \tag{22}$$

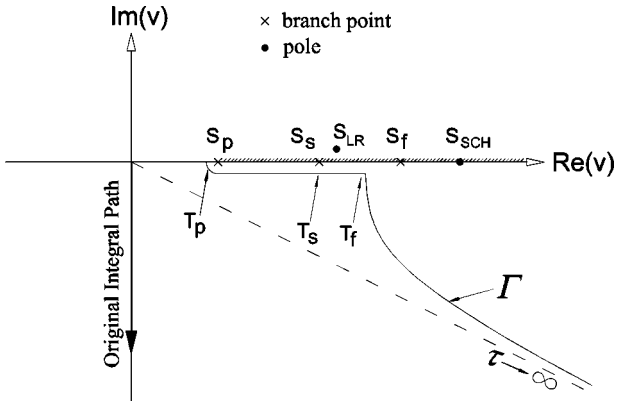

FIG. 2. Complex v plane and the modified integral path. The indices denote: P→leaky P wave, S→leaky S wave, LR→leaky R wave, f→fluid acoustic wave, SCH→Scholte wave.

where $G^P(t)$ is defined as the Green's function for pressure. The variable v is related to γ in Eq. (15) by $v = -\gamma s_S$. According to the analysis in the previous section, there are two poles in the right half complex v plane, which correspond to leaky Rayleigh and Scholte wave arrivals. The integral path along the negative imaginary axis can be deformed to path Γ as shown in Fig. 2. The new integration path Γ is defined by the equation $\tau = vr - z\sqrt{s_F^2-v^2}$, which can be solved for v to yield

$$v(\tau) = \frac{\tau r + z\sqrt{s_F^2R^2-\tau^2}}{R^2}, \quad \tau \text{ is real and } 0 \leqslant \tau \leqslant \infty, \tag{23}$$

where $R = \sqrt{r^2+z^2}$. The benefit of deforming the original integration path to Γ is obvious, because there is no pole along the new path. The Green's function integration along the new path is

$$G^P(t) = \left(\mathrm{Im}\int_{t_p}^t \frac{\sqrt{s_P^2-v(\tau)^2}}{\sqrt{s_F^2-v(\tau)^2}}\frac{v(\tau)}{D[iv(\tau)]} \times \frac{r - \tau z/\sqrt{s_F^2R^2-\tau^2}}{R^2\sqrt{[t-\tau+v(\tau)r]^2-v(\tau)^2r^2}}d\tau\right), \tag{24}$$

where $t_p = rs_P + |z|\sqrt{s_F^2-s_P^2}$ is the leaky P wave arrival time. $G^P(t) = 0$ when $t < t_p$.

However, when the receiver is located on the interface, i.e., $z = 0$, the integral path Γ is along the real axis, and passes by the Scholte pole. In this case, the principal value of Eq. (24) must be taken.

The integrand in Eq. (24) has a square root singularity at end point $\tau = t$, which increases the difficulty of numerical integration. This problem can be solved by further introducing the following transformation,

$$\tau = t_1\cos^2(\theta) + t_2\sin^2(\theta), \tag{25}$$

where t_1, t_2 are the lower and upper limits of the integration. Then the integration interval $t_1 \leqslant \tau \leqslant t_2$ is mapped to the fixed interval $0 \leqslant \theta \leqslant \pi/2$, while

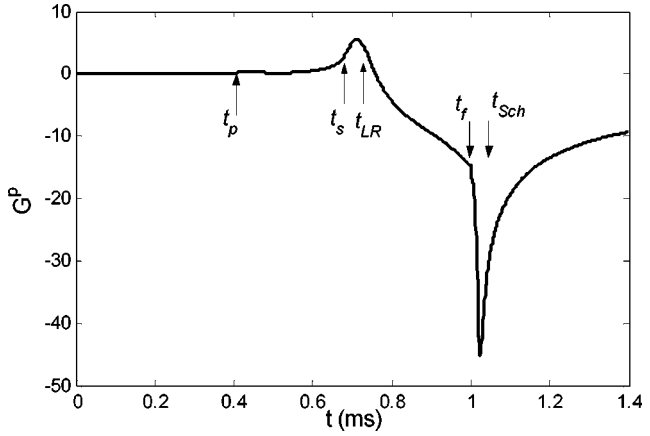

FIG. 3. Green's function $G^P(t)$ for pressure in the fluid at position $r=1.5$ m, $z=-0.05$ m. Material parameters for the fluid $\rho_1=1000$ kg/m^3, $c_F=1500$ m/s; for the solid, $\rho_2=2400$ kg/m^3, $c_P=4000$ m/s, $\upsilon=0.25$.

$$d\tau=2(t_2-t_1)\sin(\theta)\cos(\theta),$$

$$\sqrt{[t_2-\tau+v(\tau)r]^2-v(\tau)^2r^2}$$
$$=\sqrt{(t_2-t_1)}\cos(\theta)\sqrt{(t_2-t_1)\cos^2(\theta)+2v(\tau)r}. \quad (26)$$

Another square root singularity at point $\tau=t_f=s_FR$ can be processed similarly. A similar technique was also used by de Hoop (1984).

The vertical component of displacement in the fluid is also obtained in the same way:

$$w(t)=-\frac{Q}{\pi^2}\frac{s_S^4}{\rho_2}\mathrm{Im}\int_{t_p}^{t}\frac{\sqrt{s_P^2-v(\tau)^2}v(\tau)}{D[iv(\tau)]R^2}$$
$$\times\frac{r-\tau z/\sqrt{s_F^2R^2-\tau^2}}{\sqrt{[t-\tau+v(\tau)r]^2-v(\tau)^2r^2}}d\tau. \quad (27)$$

Figure 3 shows the Green's function $G^P(t)$ at a near-surface position $r=1.5$ m, $z=-0.05$ m in the fluid. The material configuration simulates a concrete/water system. The arrival times of all wave types are marked. It is noticed that the slope is discontinuous at positions $t=t_p$, t_s, and t_f, which correspond to the leaky P-, leaky S-, and fluid acoustic waves in water. From the mathematics viewpoint, these discontinuities come from the branch points along the integral path Γ. The poles corresponding to the leaky Rayleigh and Scholte wave arrivals contribute to the large smooth peaks. When the receiving position is very close to the interface, the integral path Γ in Fig. 2 will bend to the real axis, and a sharp peak will appear nearby the Scholte wave arrival in Fig. 3.

The impulse response to a point loading on the interface between a fluid and a solid half-space can be obtained from the corresponding step response solution by taking differentiation with respect to time. Then for any transient loading that has arbitrary temporal variation and spatial distribution, the response can be obtained by convolving the impulse response in both time and space domains.

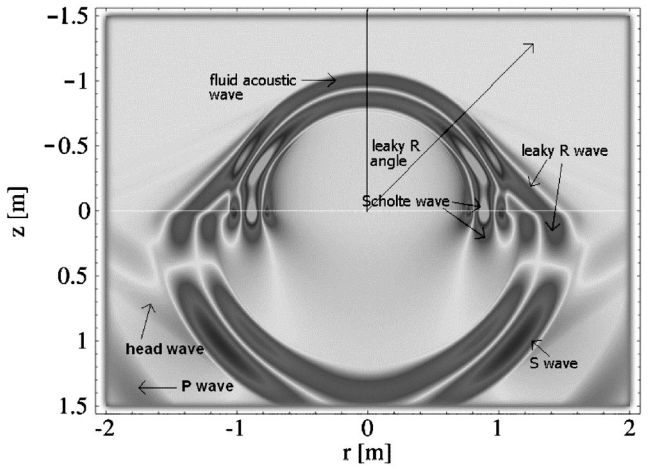

FIG. 4. Absolute value of pressure (in fluid) and stress τ_{zz} (in solid) field snapshot at $t=0.72$ ms given by EFIT analysis. The interface is subject to a transient point load that varies with time as $f(t)=\sin^2(\pi t/T)$ with $T=200$ μs.

V. VERIFICATION BY NUMERICAL SIMULATION

To verify the obtained analytical solutions, numerical analyses were performed to simulate the response for fluid–solid half-space cases. The elastodynamic finite integration technique (EFIT) is a numerical time-domain scheme to model elastic wave propagation in homogeneous and heterogeneous, dissipative and nondissipative, as well as isotropic and anisotropic elastic media (Fellinger *et al.*, 1995). EFIT uses a velocity-stress formalism on a staggered spatial and temporal grid complex. The starting point of EFIT is the integral form of the linear governing equations, i.e., the Cauchy equation of motion, and the equation of deformation rate. EFIT performs integrations over certain control volumes V, and the surfaces of these cells S, assuming constant velocity and stress within V and on each S. This method requires staggered grids and leads to a very stable and efficient numerical code, which also allows easy and flexible treatment of various boundary conditions. In recent years, EFIT has been successfully used for a wide variety of applications, especially in the field of nondestructive testing (Schubert and Marklein, 2003).

In the present case of a transient point load at a fluid–solid interface, we used a special axisymmetric EFIT code in cylindrical coordinates (Schubert *et al.*, 1998). The water/concrete case shown in Fig. 3 was studied. The material parameters are for water, $\rho_1=1000$ kg/m^3, $c_F=1500$ m/s, and for concrete $\rho_2=2400$ kg/m^3, P wave velocity $c_P=4000$ m/s, and Poisson's ratio $\nu=0.25$. The vertical transient point load varies with time as function $f(t)=\sin^2(\pi t/T)$, where the force duration is $T=200$ μs. A grid spacing of $\Delta r=\Delta z=2.5$ mm and a time step of 0.44 μs are used in order to guarantee stability as well as sufficient discretization of the shortest wavelengths. The dimensions of the model are 2 m in radial and 3 m in axial direction, resulting in 800×1200 grid cells. At the outer boundaries of the model, highly effective absorbing boundary conditions based on the perfectly matched layer (PML) are used in order to suppress interfering reflections (Liu, 1999).

Figure 4 shows the cross-sectional snapshot image of

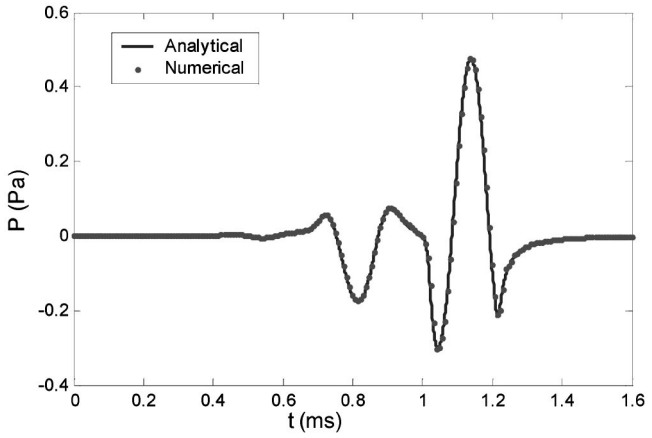

FIG. 5. Comparison of the analytical and the numerical solutions for pressure in the fluid at $r=1.5$ m, $z=-0.05$ m. The interface is subject to a point load that varies with time as $f(t)=\sin^2(\pi t/T)$ with $T=200\ \mu$s. Material parameters for the fluid $\rho_1=1000\ \mathrm{kg/m^3}$, $c_F=1500$ m/s; for the solid $\rho_2=2400\ \mathrm{kg/m^3}$, $c_P=4000$ m/s, $v=0.25$.

pressure field (absolute value) as generated by EFIT, at time $t=0.72$ ms. Only the region with $r>0$ was calculated, but for better illustration the reversed region with $r<0$ is also shown here. The half-circle in the upper half-plane represents the acoustic wave front in water, and the inclined lines represent the leaky Rayleigh wave fronts, which are tangent to the half circle at the leaky angle direction. In this case, the leaky Rayleigh angle determined by Snell's law is $\theta=43.8°$, measured from the vertical axis. The leaky Rayleigh wave front is separable from the subsequent Scholte and fluid acoustic wave fronts at larger values of radial distance r. The 3-D shape of the combined leaky Rayleigh and fluid acoustic wave fronts looks like a domed cone. The leaky Rayleigh wave in concrete is also seen, which behaves similarly to the ordinary Rayleigh wave, and attenuates exponentially with increasing depth in the solid. In the near-interface region, the Scholte wave effect is strong in both the fluid and the solid.

Figure 5 shows the analytical and numerical time domain near-surface response of the pressure in water, at position $r=1.5$ m, $z=-0.05$ m. Very good agreement between analytical and numerical responses is observed.

VI. SIMPLIFIED LEAKY RAYLEIGH WAVE RESPONSE

In Sec. IV, the complete analytical solution of pressure and displacement in the fluid are obtained. However, the integral form solution is not always convenient to use. In this and the next sections, the authors provide a simplified closed-form solution to the same problem by considering only Rayleigh and Scholte pole contributions. This simplification is acceptable when measurements are taken at a large distance from the source.

According to the previous analysis, the wave field excited by a normal point load at the interface includes contributions from leaky P, S, Rayleigh, fluid acoustic, and Scholte waves. Analysis shows that, at large horizontal distances from the source, disturbances near the interface are dominated by leaky Rayleigh and Scholte wave contributions, which can be obtained from the residues at corresponding poles. The similar idea was already used to investigate Rayleigh wave effects in a free surface half-space by Chao *et al.* (1961). Achenbach (1973) reproduced Chao's results in detail. The simplified solution provides an easy and quick way to estimate leaky Rayleigh and Scholte wave effects.

A. Displacements and stresses in the fluid

Applying the inverse Hankel and Laplace transforms to the transformed solution in Eq. (13), the pressure in fluid can be expressed as

$$P(r,z,t)=-\frac{Q}{2\pi}\frac{s_S^4}{2\pi i}\frac{\rho_1}{\rho_2}\int_0^\infty J_0(\xi r)\xi \times\int_{\epsilon-i\infty}^{\epsilon+i\infty}\frac{\alpha_2}{\alpha_1}\frac{p^3}{D_H(\xi,p)}e^{\alpha_1 z+pt}\,dp\,d\xi. \tag{28}$$

Considering the integrand term, the contributions from the leaky Rayleigh poles are

$$I_1=\frac{1}{2\pi i}\int_0^\infty J_0(\xi r)\xi\int_{\epsilon-i\infty}^{\epsilon+i\infty}\frac{\alpha_2}{\alpha_1}\frac{p^3}{D_H(\xi,p)}e^{\alpha_1 z+pt}\,dp\,d\xi =\int_0^\infty J_0(\xi r) \times\xi\left[\frac{\alpha_2}{\alpha_1}\frac{p^3}{\partial D_H(\xi,p)/\partial p}e^{\alpha_1 z+pt}\right]_{p=i\xi/s_S\gamma_{R1},\,i\xi/s_S\gamma_{R2}}d\xi, \tag{29}$$

where the expression $[(\alpha_2/\alpha_1)\times[p^3/\partial D_H(\xi,p)/\partial p]]_{p=i\xi/s_S\gamma_{R1},\,i\xi/s_S\gamma_{R2}}$ represents a pair of complex conjugate constants, denoted as A_1 and $\overline{A_1}$.

Introducing

$$m_{1,2}=-\frac{i}{\gamma_{R1,R2}}\left[\frac{z}{r}\sqrt{u^2-\gamma_{R1,R2}^2}+\frac{t}{s_S r}\right] \tag{30}$$

generates

$$[\alpha_1 z+pt]_{p=i\xi/s_S\gamma_{R1,R2}}=-\xi r m_{1,2}, \tag{31}$$

where $m_1=\overline{m_2}$. Thus, Eq. (29) can be expressed as

$$I_1=A_1\int_0^\infty J_0(\xi r)\xi e^{-\xi m_1 r}d\xi+\overline{A_1}\int_0^\infty J_0(\xi r)\xi e^{-\xi m_2 r}\,d\xi =2\,\mathrm{Re}\int_0^\infty A_1 e^{-\xi m_1 r}J_0(\xi r)\xi\,d\xi =\frac{2}{r^2}\mathrm{Re}\left[\frac{A_1 m_1}{(1+m_1^2)^{3/2}}\right],\quad \mathrm{Re}(m_1)>0, \tag{32}$$

where we use the zeroth-order Hankel transform formula

$$\int_0^\infty J_0(\xi r)\xi e^{-a\xi}\,d\xi=\frac{a}{(r^2+a^2)^{3/2}},\quad \mathrm{Re}(a)>0. \tag{33}$$

From Eq. (28), the pressure P is expressed as

$$P=-\frac{Q}{\pi}\frac{\rho_1}{\rho_2}\frac{1}{r^2}s_S^4\,\mathrm{Re}\left[\frac{A_1 m_1}{(1+m_1^2)^{3/2}}\right]. \tag{34}$$

Similarly, by introducing

$$A_2=\xi\left[\frac{\alpha_2 p}{\partial D_H(\xi,p)/\partial p}\right]_{p=i\xi/s_S\gamma_{R1}},$$
$$A_3=\left[\frac{\alpha_2}{\alpha_1}\frac{p\xi^2}{\partial D_H(\xi,p)/\partial p}\right]_{p=i\xi/s_S\gamma_{R1}}, \tag{35}$$

the vertical and radial components of the displacement in the fluid are obtained:

$$w_1=\frac{Q}{\pi}\frac{s_S^4}{\rho_2}\frac{1}{r}\mathrm{Re}\left[\frac{A_2}{(1+m_1^2)^{1/2}}\right],$$
$$u_1=-\frac{Q}{\pi}\frac{s_S^2}{\mu}\frac{1}{r}\mathrm{Re}\left(\left[1-\frac{m_1}{(1+m_1^2)^{1/2}}\right]A_3\right), \tag{36}$$
$$\mathrm{Re}(m_1)>0.$$

Care should be taken with the square root when calculating $m_{1,2}$ from Eq. (30). To have bounded results, only the branch that gives $\mathrm{Re}(m_1)>0$ should be selected.

B. Displacement and stress in the solid half-space

The response of the leaky Rayleigh wave in the solid can be obtained in a similar way. Introducing

$$n_{p1,2}=\frac{1}{\gamma_{R1,R2}}\left[\pm\frac{z}{r}\sqrt{\gamma_{R1,R2}^2-q^2}-i\tau\right],$$
$$n_{s1,2}=\frac{1}{\gamma_{R1,R2}}\left[\pm\frac{z}{r}\sqrt{\gamma_{R1,R2}^2-1}-i\tau\right] \tag{37}$$

yields

$$[-\alpha_2 z+pt]_{p=i\xi/s_S\gamma_{R1,R2}}=-\xi\frac{r}{\gamma_{R1,R2}}\left[\pm\sqrt{\gamma_{R1,R2}^2-q^2}\frac{z}{r}-i\tau\right]=-\xi r n_{p1,2},$$
$$[-\beta z+pt]_{p=i\xi/s_S\gamma_{R1,R2}}=-\xi\frac{r}{\gamma_{R1,R2}}\left[\pm\sqrt{\gamma_{R1,R2}^2-1}\frac{z}{r}-i\tau\right]=-\xi r n_{s1,2}. \tag{38}$$

The real part of Eq. (38) must be negative to have bounded responses, therefore the real parts of n_{p1}, n_{p2}, n_{s1}, n_{s2} must be positive. Using the similar argument for dealing with $m_{1,2}$, only those results of n_{p1}, n_{p2}, n_{s1}, n_{s2} that have positive real parts are acceptable. In addition, n_{p1}, n_{p2} and n_{s1}, n_{s2} should be complex conjugate pairs.

Applying the inverse Hankel and Laplace transforms to Eq. (14) and calculating the residues at Rayleigh poles yields the displacements and stresses in the solid,

$$w_2=\frac{Q}{\pi}\frac{s_S^2}{\rho_2}\frac{1}{r}\mathrm{Re}\left[\frac{B_1}{\sqrt{1+n_{p1}^2}}-\frac{B_2}{\sqrt{1+n_{s1}^2}}\right],$$
$$u_2=\frac{Q}{\pi}\frac{s_S^2}{\rho_2}\frac{1}{r}\mathrm{Re}\left[B_3\left(1-\frac{n_{p1}}{\sqrt{1+n_{p1}^2}}\right)-B_4\left(1-\frac{n_{s1}}{\sqrt{1+n_{s1}^2}}\right)\right], \tag{39}$$
$$\tau_{zz2}=-\frac{Q}{\pi}\frac{1}{r^2}\mathrm{Re}\left[\frac{B_5 n_{p1}}{(1+n_{p1}^2)^{3/2}}-\frac{B_6 n_{s1}}{(1+n_{s1}^2)^{3/2}}\right],$$
$$\tau_{zr2}=\frac{Q}{\pi}\frac{1}{r^2}\mathrm{Re}\left[\frac{-B_7}{(1+n_{p1}^2)^{3/2}}+\frac{B_7}{(1+n_{s1}^2)^{3/2}}\right],$$

where the coefficients are

$$B_1=\left[\frac{s_S^2p^2+2\xi^2}{p\partial D_H(\xi,p)/\partial p}\alpha_2\xi\right]_{p=i\xi/s_S\gamma_{R1}},$$
$$B_2=\left[\frac{2\xi^3\alpha_2}{p\partial D_H(\xi,p)/\partial p}\right]_{p=i\xi/s_S\gamma_{R1}},$$
$$B_3=\left[\frac{(s_S^2p^2+2\xi^2)}{p\partial D_H(\xi,p)/\partial p}\xi^2\right]_{p=i\xi/s_S\gamma_{R1}}, \tag{40}$$
$$B_4=\left[\frac{2\xi^2\alpha_2\beta}{p\partial D_H(\xi,p)/\partial p}\right]_{p=i\xi/s_S\gamma_{R1}},$$
$$B_5=\left[\frac{(s_S^2p^2+2\xi^2)^2}{p\partial D_H(\xi,p)/\partial p}\right]_{p=i\xi/s_S\gamma_{R1}},$$
$$B_6=2B_4,\quad B_7=2B_1.$$

The expressions in Eq. (39) are only valid in the region where $\mathrm{Re}(n_{p1,p2})>0$ and $\mathrm{Re}(n_{s1,s2})>0$. Other stress components in the solid can be derived from the following stress–displacement relations:

$$\tau_{rr2}=(\lambda_2+2\mu)\frac{\partial u_2}{\partial r}+\lambda_2\left(\frac{u_2}{r}+\frac{\partial w_2}{\partial z}\right),$$
$$\tau_{\theta\theta2}=(\lambda_2+2\mu)\frac{u_2}{r}+\lambda_2\left(\frac{\partial u_2}{\partial r}+\frac{\partial w_2}{\partial z}\right). \tag{41}$$

C. Attenuation and dispersion of leaky Rayleigh waves

In addition to the geometric decay due to the effect of point loading, which varies as $1/\sqrt{r}$ along the interface for the Rayleigh wave, there is another type of attenuation caused by continuous radiation (leakage) of energy into the fluid. In frequency domain, the solutions are exponential functions of $(-\xi r)$, where ξ has the physical meaning of wavenumber. According to Eq. (32), higher frequency (larger ξ) contents give more attenuation during propagation. Therefore the waveform generated by a transient loading becomes wider with increasing distance, i.e., it shows dispersion property due to leakage-induced attenuation, although the phase velocity of leaky Rayleigh waves does not vary with frequency.

VII. SCHOLTE WAVE RESPONSE

The real roots of the Scholte equation correspond to Scholte wave propagation along the interface. The Scholte wave solutions can be obtained by calculating the residues at the poles $\gamma=\pm\gamma_{sch}$. For common cases of light fluids lying

on stiff solids, the root $|\gamma_{sch}| = s_{sch}/s_S$ is slightly larger than $u = s_F/s_S$. Therefore, Eqs. (31) and (38) are changed to

$$
\begin{aligned}
&[\alpha_1 z + pt]_{p=i\xi/\pm s_S\gamma_{sch}} = -\xi r m_{1,2}^{sch},\\
&[-\alpha_2 z + pt]_{p=i\xi/\pm s_S\gamma_{sch}} = -\xi r n_{p1,2}^{sch},\\
&[-\beta z + pt]_{p=i\xi/\pm s_S\gamma_{sch}} = -\xi r n_{s1,2}^{sch},
\end{aligned}
\tag{42}
$$

where

$$
\begin{aligned}
m_{1,2}^{sch} &= -\frac{1}{\gamma_{sch}}\left(\sqrt{\gamma_{sch}^2 - u^2}\frac{z}{r} \pm i\frac{t}{s_S r}\right),\\
n_{p1,2}^{sch} &= \frac{1}{\gamma_{sch}}\left(\sqrt{\gamma_{sch}^2 - q^2}\frac{z}{r} \pm i\frac{t}{s_S r}\right),\\
n_{s1,2}^{sch} &= \frac{1}{\gamma_{sch}}\left(\sqrt{\gamma_{sch}^2 - 1}\frac{z}{r} \pm i\frac{t}{s_S r}\right).
\end{aligned}
\tag{43}
$$

The solutions for the leaky Rayleigh wave are also valid for the Scholte wave by substituting m^{sch}, n_p^{sch}, and n_s^{sch} for m, n_p, and n_s. The first terms in the expressions of Eq. (43) represent the real parts, which are positive and result in the decay in z direction. It can be seen that the Scholte wave decays exponentially in z direction in both the fluid and the solid. For lighter fluid cases, i.e., where the acoustic impedance of the fluid is less than that of the solid, $\sqrt{\gamma_{sc}^2 - u^2}$ is much smaller than $\sqrt{\gamma_{sc}^2 - q^2}$ and $\sqrt{\gamma_{sc}^2 - 1}$. This indicates that the Scholte wave attenuates much more quickly in the solid than in the fluid. Therefore, in contrast to the leaky Rayleigh wave, most of Scholte wave energy is localized in the fluid (Gusev *et al.*, 1996). The Scholte wave generation efficiency increases with increasing acoustic impedance of the fluid. For example, it is much easier to generate Scholte waves in the water/concrete configuration than the air/concrete configuration. In fact, almost no Scholte wave effect can be observed in the air/concrete case. With increasing impedance of the fluid, Scholte waves have deeper penetration depth in the solid. This property provides the possibility for NDT application of Scholte waves, which was studied experimentally by Glorieux *et al.* (2001). Because there is no leakage during Scholte wave propagation along the radial direction, the decay in the radial direction is only attributed to the geometrical effect. In 2-D cases, the Scholte wave travels without attenuation along the propagation direction (Glorieux *et al.*, 2001).

VIII. COMPARISON OF THE EXACT AND SIMPLIFIED SOLUTIONS

Figure 6 shows the comparison of the exact and simplified analytical solutions for fluid pressure for the water/concrete case. In Fig. 6(a), when the receiver position is close to the interface ($r = 1.5$ m, $z = -0.05$ m), good agreement is observed around the leaky Rayleigh and Scholte wave arrival times. The small yet noticeable differences before the leaky Rayleigh and Scholte wave arrivals are due to the absence of leaky body waves and fluid acoustic waves in the simplified solution. When the receiver is away from the interface, as shown in Fig. 6(b) for receiver position $r = 1.5$ m, $z = -0.5$ m, the degree of agreement between the simplified and exact analytical solutions decreases. Generally speaking, the simplified solution provides better estimation of pressure for larger r and smaller $|z|$ cases, where the contribution of body waves is negligible.

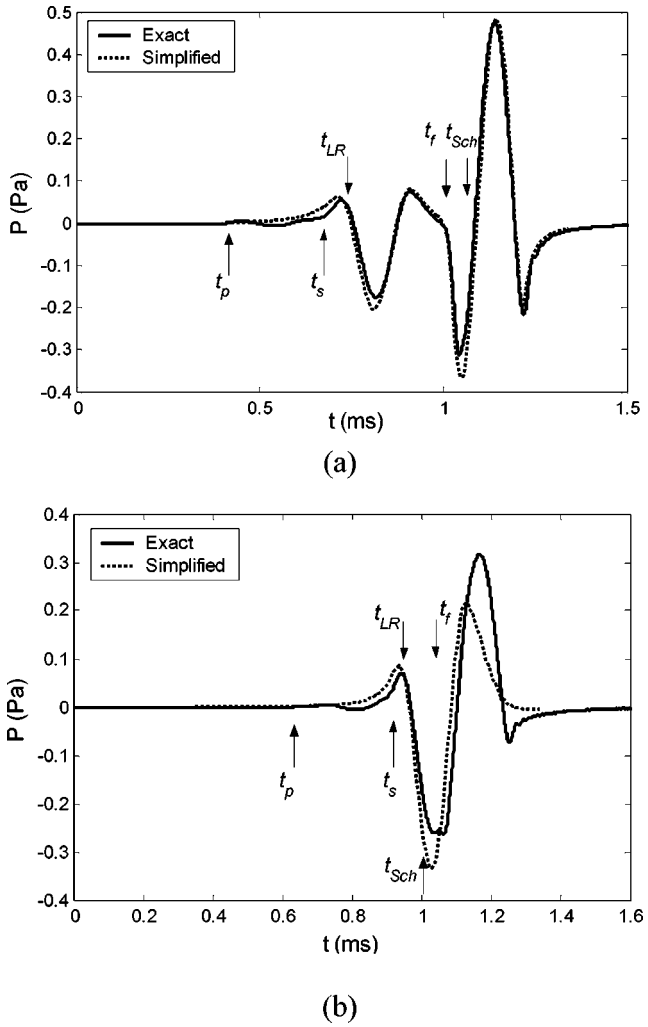

FIG. 6. Comparison of the exact and simplified solutions for water/concrete case. Pressure in the fluid at position (a) $r = 1.5$ m, $z = -0.05$ m, and (b) $r = 1.5$ m, $z = -0.5$ m. The interface is subject to a point load that varies with time as $f(t) = \sin^2(\pi t/T)$ with $T = 200$ μs. Material parameters for the fluid $\rho_1 = 1000$ kg/m^3, $c_F = 1500$ m/s; and for the solid $\rho_2 = 2400$ kg/m^3, $c_P = 4000$ m/s, $v = 0.25$.

Figures 7(a) and (b) show the comparison of the exact and simplified solutions for the air/concrete case. The receiver positions are $r = 1.0$ m, $z = -0.05$ m and $r = 1.0$ m, $z = -0.5$ m, respectively. Good agreement is observed near the leaky Rayleigh wave arrival time for both positions, while obvious differences can be seen near the Scholte and fluid acoustic wave arrival times. The reason is that the leaky Rayleigh wave is well separated from the fluid acoustic wave, and Scholte wave contribution is very small compared to the acoustic wave contribution in the fluid for air/concrete case, even in the near-interface region. Therefore, for the air/concrete configuration, the pressure field in the fluid is dominated by leaky Rayleigh and fluid acoustic waves. In air-coupled sensing, the leaky Rayleigh wave is usually the component in which we are interested. The acoustic wave contribution in the fluid can be separated by increasing mea-

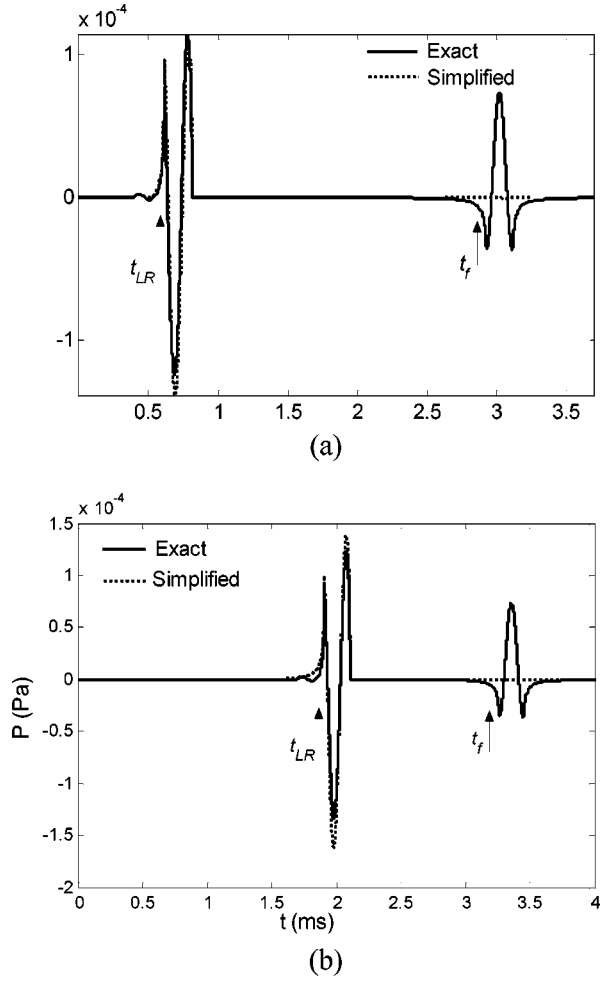

FIG. 7. Comparison of the exact and simplified solutions for air/concrete case. Pressure in the fluid at position (a) $r=1.0$ m, $z=-0.05$ m, and (b) $r=1.0$ m, $z=-0.5$ m. The interface is subject to a point load that varies with time as $f(t)=\sin^2(\pi t/T)$ with $T=200$ μs. Material parameters for the fluid $\rho_1=1.21$ kg/m^3, $c_F=343$ m/s; for the solid $\rho_2=2400$ kg/m^3, $c_P=4000$ m/s, $\nu=0.25$.

suring distance r between receivers and the source, or eliminated by employing the directional property of the air-coupled sensor (Zhu *et al.*, 2001).

The excitation effectiveness of leaky Rayleigh waves induced by an impact point load can be inferred from Fig. 7. For a typical impulse force $f(t)=\sin^2(\pi t/T)$ with a modest peak value of 1 kN and duration $T=200$ μs, the output pressure of the leaky Rayleigh wave is 0.1–0.15 Pa, which is approximately equivalent to a sound pressure level of 75 dB. Such a pressure is large enough to be detected readily by an air-coupled sensor, even when material attenuation effects are considered. The excitation effectiveness of leaky Rayleigh waves is dependent on the impact force duration. Shorter force durations give higher output pressure of leaky Rayleigh waves. For example, when the duration is decreased to $T=50$ μs, the output peak pressure of the leaky Rayleigh wave will increase to 1.2 Pa (95 dB). Most impactors used for concrete testing will generate transient forces with duration between 50 and 200 μs.

IX. CONCLUSIONS

The exact analytical solution to the ''Lamb'' problem in a fluid/solid half-space system is derived by the Cagniard–de Hoop method. Simplified formulations are also derived, which provide an easy and quick way to estimate leaky Rayleigh and Scholte wave contributions. The following conclusions can be drawn based on the analysis:

(1) A transient point load applied to the interface is an effective way to generate leaky Rayleigh waves in the fluid. For air-coupled wave detection in concrete, the excitation effectiveness of leaky Rayleigh waves is around 0.1–1.0 Pa/kN, depending on the impact force duration.
(2) For the light fluid/heavy solid case, the leaky Rayleigh wave is separable from Scholte and acoustic waves in the fluid when distance r is large enough, where r depends on velocities of leaky Rayleigh, Scholte, and acoustic waves, vertical distance $|z|$, and force duration. For the air–concrete configuration shown in Fig. 7(a), where $|z|=0.05$ m and $r>0.2$ m, the difference in arrival time between leaky Rayleigh and acoustic waves is >362 μs. Therefore the received signals will be dominated by leaky Rayleigh waves, which provide important material information of the underlying solid.
(3) Simplified solutions are obtained when contributions from leaky Rayleigh waves and Scholte waves poles only are considered. Equations (34)–(36) and (39) give the solution to responses in the fluid and solid, respectively. The simplified solution accurately simulates the transient pressure field response for the air/concrete case when the fluid acoustic wave contribution is removed or separated.
(4) The Scholte wave contribution is prominent in the near-interface region for the water/concrete case. Because most of the energy of Scholte waves is localized in the fluid, however, Scholte wave properties are not very sensitive to the variation of the underlying solid materials, which limits the NDE application of Scholte waves for the common light fluid/heavy solid cases.

ACKNOWLEDGMENTS

This work was carried out in the course of research sponsored by the National Science Foundation under Grant No. 0223819. The authors also wish to thank Dr. Nelson Hsu from National Institute of Standards and Technology for his helpful suggestions.

Achenbach, J. D. (**1973**). *Wave Propagation in Elastic Solids* (North-Holland, Amsterdam, The Netherlands), Chap. 7, pp. 262–321.
Castaings, M., and Hosten, B. (**2001**). ''Lamb and SH waves generated and detected by air-coupled ultrasonic transducers in composite material plates,'' NDT & E Int. **34**, 249–258.
Chao, C. C. (**1961**). ''Surface waves in an elastic half space,'' J. Appl. Mech. **28**, 300–301.
de Hoop, A. T., and van der Hijden, J. (**1983**). ''Generation of acoustic waves by an impulsive line source in a fluid/solid configuration with a plane boundary,'' J. Acoust. Soc. Am. **74**, 333–342.
de Hoop, A. T., and van der Hijden, J. (**1984**). ''Generation of acoustic waves by an impulsive point source in a fluid/solid configuration with a plane boundary,'' J. Acoust. Soc. Am. **75**, 1709–1715.
Fellinger, P., Marklein, R., Langenberg, K. J., and Klaholz, S. (**1995**). ''Numerical modelling of elastic wave propagation and scattering with EFIT—Elastodynamic finite integration technique,'' Wave Motion **21**, 47–66.
Glorieux, C., and Van de Rostyne, K. (**2001**). ''On the character of acoustic waves at the interface between hard and soft solids and liquids,'' J. Acoust. Soc. Am. **110**, 1299–1306.

Gusev, V., Desmet, C., Lauriks, W., Glorieux, C., and Thoen, J. (**1996**). ''Theory of Scholte, leaky Rayleigh, and lateral wave excitation via the laser-induced thermoelastic effect,'' J. Acoust. Soc. Am. **100**, 1514–1528.
Liu, Q. H. (**1999**). ''Perfectly matched layers for elastic waves in cylindrical and spherical coordinates,'' J. Acoust. Soc. Am. **105**, 2075–2084.
Mozhaev, V. G., and Weihnacht, M. (**2002**). ''Subsonic leaky Rayleigh waves at liquid-solid interfaces,'' Ultrasonics **40**, 927–933.
Qi, Q. (**1994**). ''Attenuated leaky Rayleigh waves,'' J. Acoust. Soc. Am. **95**, 3222–3230.
Schubert, F., and Marklein, R. (**2003**). ''Numerical Computation of Ultrasonic Wave Propagation in Concrete using the Elastodynamic Finite Integration Technique (EFIT),'' in *Proc. IEEE Ultrasonics Symp.*, Munich, Germany, 8–11 October, 2002, Article 5G-5, 778–783 (on CD).
Schubert, F., Peiffer, A., Koehler, B., and Sanderson, T. (**1998**). ''The elastodynamic finite integration technique for waves in cylindrical geometries,'' J. Acoust. Soc. Am. **104**, 2604–2614.
Viktorov, I. A. (**1967**). *Rayleigh and Lamb Waves* (Plenum, New York).
Zhu, J., and Popovics, J. S. (**2001**). ''Non-contact detection of surface waves in concrete using an air-coupled sensor,'' in *Review of Progress in Quantitative Nondestructive Evaluation* (American Institute of Physics, Melville, NY), Vol. 20B, 1261–1268.